

Finite Element Analysis of a Wind Generator with Two Counter-Rotating Rotors

Leonard Melcescu, Tiberiu Tudorache, Ovidiu Craiu

Faculty of Electrical Engineering,
University POLITEHNICA of Bucharest
Bucharest, Romania

Mihail Popescu

National Institute for R&D in Electrical Engineering,
Bucharest, Romania

Abstract—This paper presents a 2D finite element analysis of a counter-rotating permanent magnet wind generator. The studied device is a two in one electrical machine used for counter-rotating dual rotor wind turbines used to convert the wind energy into electricity. The purpose of this study is to design the machine and to estimate its behaviour using the finite element based software package Flux ®.

Keywords—counter-rotating dual rotor wind generator; permanent magnet; finite element analysis.

I. INTRODUCTION

The society development during the last century has been accompanied by a continuous growth of the overall electric energy consumption, a sign of increasing living standards. In this context, the electric energy consumption per capita has become one of the important economic indicators for the countries around the globe. Since the operation of classical electric power systems is based mainly on fossil fuels, the perspective of depletion of these resources encouraged the society to find new and efficient solutions to exploit the renewable energies (wind, solar, hydro, biomass etc.).

The wind energy represents one of the most important renewable energy resource with a high potential of conversion into electricity. The conversion of wind energy is based on wind turbines with horizontal or vertical shafts coupled to electric generators (synchronous generators or induction generators), which deliver electricity to the national power grid or to a local grid. Small power wind conversion systems are used also for storing electric energy into batteries [1]-[5].

Several solutions for increasing the conversion efficiency of wind kinetic energy into electricity have emerged. One of them supposes to increase the wind turbine power coefficient. However, from the wind turbine theory, it is known that the maximum theoretical power coefficient is limited by Betz's law. Thereby, increasing this coefficient requires special techniques. One of these techniques consists in connecting two wind rotors spinning in opposite directions, each of them driving a separate electric armature [6]-[9]. Such a solution with two wind rotors produces mechanical power equivalent to that of a single wind turbine system with a larger diameter, Fig 1. Another important advantage of the double rotor solution consists in the possibility of orienting the wind turbine blades more easily according to the wind blowing

direction. As the two wind turbines rotate in opposite directions, the relative speed between the two electric armatures is larger, the electric generator being able to produce a higher power at the same frame size, which implies a reduced consumption of active materials.

Various aspects related to the wind turbines with two counter rotating rotors were studied in the last decade, with a special focus on the aerodynamics and electromechanical design of the conversion system [10]-[13].

As far as the generator used for the double counter-rotating wind turbine is concerned, the most common solution consists of a synchronous generator with two rotating armatures. The inner armature is equipped with Permanent Magnets (PM), while the outer holds a three-phase winding. The two parts rotate in opposite directions resulting in an increased speed, and a higher output power using a compact solution. However, this solution has a drawback caused by the sliding contacts (brushes and slip rings) that are present in the high power circuit, which negatively affects the machine reliability.

II. STRUCTURE OF THE PROPOSED WIND GENERATOR

This paper presents a brushless electromechanical converter consisting of three armatures: an outer stator and two rotors (an inner rotor and a middle rotor) driven by the counter-rotating wind turbines, Fig. 2.

The inner rotor, ①, is equipped with PMs and is driven by the high speed wind turbine. The second rotor of the generator is driven by the low speed wind turbine and has two three-phase windings distributed into slots.

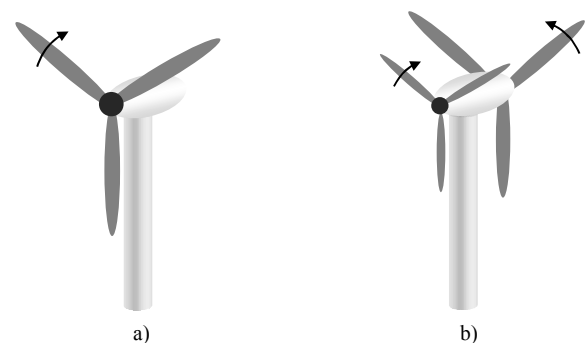


Fig. 1. Wind turbines; a) single rotor; b) two counter-rotating rotors.

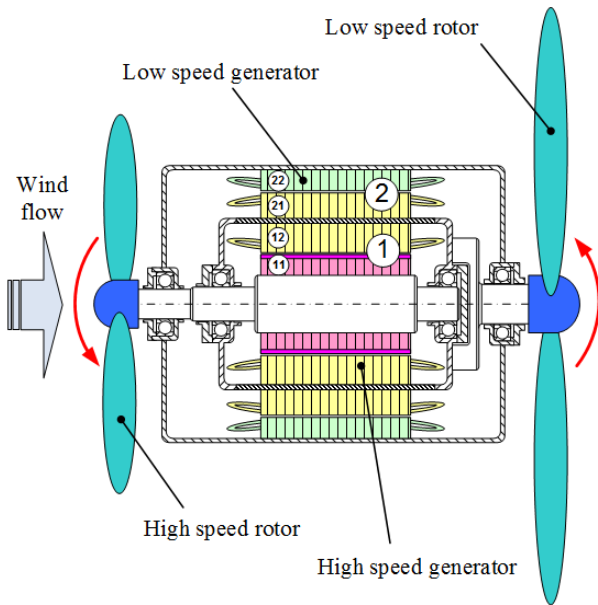


Fig. 2. Configuration of the wind generator with two counter-rotating rotors: ① - permanent magnet synchronous generator (PMSG), ⑪ - field armature of PMSG, ⑫ - coil armature of PMSG, ② - induction generator (IG), ②① - primary of IG, ②② - secondary of IG.

The inner armature, ⑫, has the same number of poles as the PM rotor, while the outer part, ②①, is equipped with a larger number of pole pairs, according the rated rotational speed. The magnetic circuits of the two three-phase windings are fixed on a non-magnetic cylinder made of steel, which is coupled to the low speed turbine.

The three-phase windings, ⑫, of the synchronous generator are connected in series with those of the induction machine, ②①, in such a way that the magnetic field produced by the later winding rotates in the same direction as the middle armature of the machine. The outer armature, ②②, represents the stator of the generator, and is equipped with a three-phase winding having a number of poles equal to that of the outer winding of the central armature, ②①. The three-phase load is connected at the terminals of the outer armature windings.

Thus, the electromechanical converter consists of two electrical machines: an inner three-phase Permanent Magnet Synchronous Generator (PMSG), ①, and an outer three-phase Induction Generator (IG), ②. The coil armature of the PMSG rotates along with the primary winding of the IG being driven by the low speed wind turbine.

Practically, the PMSG operates at a rotating speed which is equal with the sum of the rotating speeds of the two wind turbines, exploiting the fact that these turbines are counter-rotating. The IG has an inverse construction with the primary winding connected to the power supply mounted on the rotating armature and the secondary winding placed on the stator.

The electric diagram and the kinematic couplings of the wind generator are illustrated in Fig. 3. The electric power produced by the PMSG, ①, is transferred to the primary

winding of the IG, ②. The reactive power ensures the magnetization of the IG magnetic circuit and the active power is transferred to the static armature ②②. From there, partly goes to the load Z_L , and partly is converted into iron and Joule losses in the mobile armature ②①. The mechanical power produced by the low speed turbine is converted into electric power in the stator of the IG, ②②, and then is transmitted to the load.

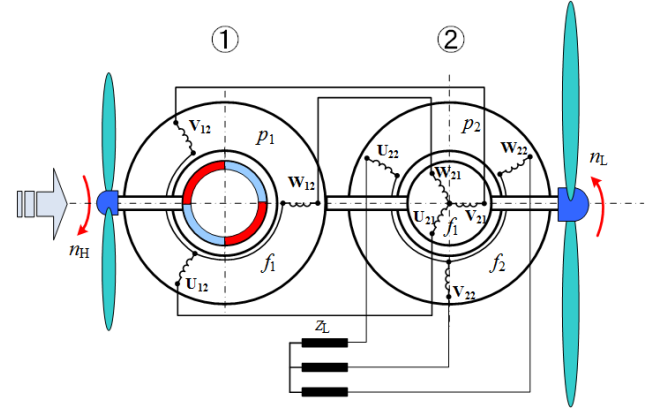


Fig. 3. Electric circuit and kinematic coupling of the wind generator.

In order to obtain the same rotational direction of the magnetic field produced by the IG three-phase primary winding, ②①, as the rotation of the middle armature, the three-phase windings of the two electric machines are connected by reversing two of their phases.

III. WIND GENERATOR OPERATION

The main components of the wind generator with two counter-rotating rotors are depicted in Fig. 4 where a cross-section of the machine is shown.

Let us consider that PMSG, ①, has p_1 pole pairs and its inductor, ⑪, is driven by the high speed turbine with clockwise rotational speed n_H , considered negative.

The three-phase winding of the PMSG, ⑫, placed on the middle armature is driven by the low speed wind turbine in the opposite direction, with the counter clockwise speed n_L , considered positive. Thus, the PMSG rotational speed, n_1 , will be equal with the difference between the two speeds, as follows:

$$n_1 = n_L - n_H. \quad (1)$$

If the speeds of the two turbines are expressed in rpm, the frequency of the induced voltage in the three-phase winding of the PMSG is given by the expression:

$$f_1 = \frac{p_1 n_1}{60} = \frac{p_1}{60} (n_L - n_H). \quad (2)$$

The IG, ②, has p_2 pole pairs and its speed, n_2 , is equal to that of the wind turbine that drives the middle armature, n_L .

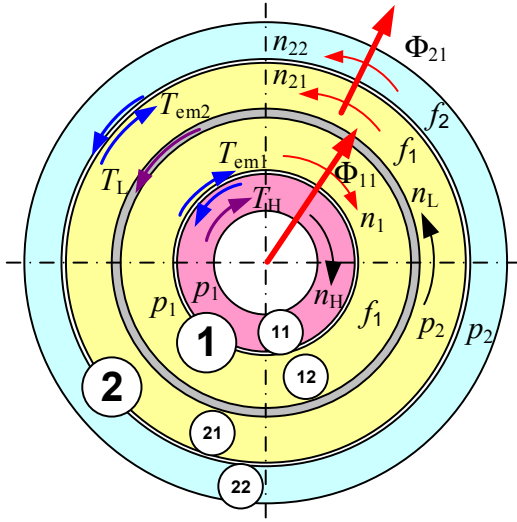


Fig. 4. Basic elements of wind generator with two counter rotating rotors: ① - permanent magnet synchronous generator (PMSG), ⑪ - field armature of PMSG, ⑫ - coil armature of PMSG, ② - induction generator (IG), ②① - primary of IG, ②② - secondary of IG.

The primary three-phase winding, ②①, is supplied from a voltage source with frequency f_1 provided by the PMSG, Fig. 3. Therefore, the currents with frequency f_1 flowing through the three-phase winding, ②①, produce a rotating magnetic field, Φ_{21} , that rotates with the speed n_{21} against the middle armature, (3), respectively with n_{22} with respect to the stator, (4). This time- and space- variable magnetic field will induce in the stator three-phase winding, ②②, voltages with frequency f_2 given by expression (5).

$$n_{21} = \frac{60f_1}{p_2} = \frac{p_1}{p_2}(n_L - n_H), \quad (3)$$

$$n_{22} = n_{21} + n_L = \frac{p_1}{p_2}(n_L - n_H) + n_L, \quad (4)$$

$$f_2 = \frac{p_2}{60} n_{22} = \frac{p_2}{60} \left(\frac{60f_1}{p_2} + n_L \right) = f_1 + \frac{p_2}{60} n_L. \quad (5)$$

According to the above equations, the synchronous speed of the induction machine will be equal to n_{21} , the speed of the rotating magnetic field produced by primary winding ②①. For an observer placed on the middle armature, the induction stator is moving in opposite direction with speed $n_2 = -n_L$. Thereby, the slip of the induction machine (6) will be greater than one, which means the machine operates as an electromagnetic brake. That is, the machine receives electrical power from the synchronous generator through its terminals ②① and mechanical power from the wind turbine which rotates with speed n_L . This way, the received power, after deducting the losses, is transferred to the load Z_L connected in the secondary circuit ②②, Fig. 3.

$$s = \frac{n_{21} + n_L}{n_{21}}. \quad (6)$$

When operating under load condition, the two electrical machines produce electromagnetic torques. At steady state, neglecting friction torque, these torques will equal those produced by the wind turbines. Therefore, the moving torque T_H produced by the turbine which moves with higher speed n_H will equal the torque T_{em1} produced by the PMSG, (7). On the middle armature that holds the PMSG three-phase winding, ②①, and the primary windings of the IG, ②①, both electromagnetic torques produced by the two electrical machines will be applied. The sum of these torques equals the mechanical torque T_L produced by the second turbine, (8).

$$T_H = T_{em1}, \quad (7)$$

$$T_L = T_{em1} + T_{em2}. \quad (8)$$

Based on a sign convention chosen for depicting the speed direction, the torque provided by the turbine which moves with negative speed n_H will be also negative ($T_H < 0$), while the torque produced by the other turbine will be positive ($T_L > 0$). Mechanical power P_1 , received by PMSG and mechanical power P_2 , received by induction machine can be expressed by the relations (9) and (10):

$$P_1 = -T_H \frac{2\pi}{60} (n_L - n_H), \quad (9)$$

$$P_2 = (T_L + T_H) \frac{2\pi}{60} n_L. \quad (10)$$

Under the assumption of zero friction losses, the total mechanical power received by the two-rotor wind generator is equal with the sum of the powers received from the two turbines, as follows:

$$P_1 + P_2 = T_H \frac{2\pi}{60} n_H + T_L \frac{2\pi}{60} n_L. \quad (11)$$

Using the symbols from Fig. 4, as explained above, the active power induced in the secondary circuit of the induction machine, P_{22} , has two components: one coming from the active power received from the synchronous generator, P_{em2} , and the other given by the mechanical power P_{m2} , received from the turbine that spins with speed n_L :

$$P_{22} = P_{em2} + P_{m2} = T_{em2} \frac{2\pi}{60} n_{21} + T_{em2} \frac{2\pi}{60} n_L, \quad (12)$$

$$P_{22} = T_{em2} \frac{2\pi}{60} (n_{21} + n_L) = s T_{em2} \frac{2\pi}{60} n_{21} = s P_{em2}.$$

In order to achieve an optimal design of the generator, the ratio between the two power components P_{em2} and P_{m2} , must be properly considered, (13).

$$\frac{P_{m2}}{P_{em2}} = \frac{P_{22} - P_{em2}}{P_{em2}} = \frac{s P_{em2} - P_{em2}}{P_{em2}} = s - 1. \quad (13)$$

The power produced by PMSG is transferred to the load through the IG windings, generating Joule losses in both machines. It is thus recommended that mechanical power P_{m2} received by the IG from the mover be larger than the active power P_{em2} taken from the PMSG. This way, the amount of Joule losses developed in the IG windings will be smaller for a given output power.

Knowing the speeds of the two turbines and using eq. (13) along with relations (1) – (6), the suitable number of pole pairs of the two electrical machines can be determined.

IV. ANALYSIS OF THE WIND GENERATOR OPERATION BY FEM

The complexity of the electromagnetic and geometric structure of the PMSG and IG and their special electric connections require a simultaneous study of the two machines. An analysis taking into account the design aspects as well as the special windings connections of the counter rotating wind generator is complex and difficult to achieve analytically. That is why our investigation used a numerical model based on Flux® software package that combines the Finite Element Method (FEM) for field computation with circuit equations [14].

The purpose of the 2D numerical analysis presented in this paper is to ensure a proper design of the machines (PMSG and IG) operating simultaneously, as well as to estimate their behaviour in various operation conditions.

A. Description of the Main Data of Studied Generator

The numerical model was developed for a wind generator with two counter-rotating rotors with total rated power $P_n = 7$ kW, when operating on a resistive-inductive load with a power factor $\cos(\phi_L) = 0.95$.

The inner rotor equipped with PMs is driven by a wind turbine with rated speed $n_H = 600$ rpm and the middle rotor is driven by a wind turbine with rated speed $n_L = 300$ rpm.

In Fig. 5 is shown half of the wind generator cross-section. The symbols used to denote the generator armatures are the same as the ones presented in Fig. 2 and Fig. 4. The synchronous generator has $2p_1 = 4$ poles and NdFeB PMs placed on the surface of the inductor and radially magnetized. The PMSG armature coil ⑫ has a double layer three-phase winding, with shortened pitch, $w_{12} = 216$ turns per phase and $q_{12} = 3$ slots per pole and phase. The IG has $2p_2 = 16$ poles, and the primary and secondary three-phase windings, ⑪ and ⑫ respectively, are double layered, short pitched and have $w_{21} = 448$ turns, and $w_{22} = 256$ turns, respectively. The primary winding has $q_{21} = 1$ and the secondary $q_{22} = 2$ slots per phase and pole.

At rated speed, the operating frequencies are $f_1 = 30$ Hz in the middle armature and $f_2 = 70$ Hz in the stator. To have reduced iron losses, the cores are made of FeSi laminations of 0.35 mm thickness.

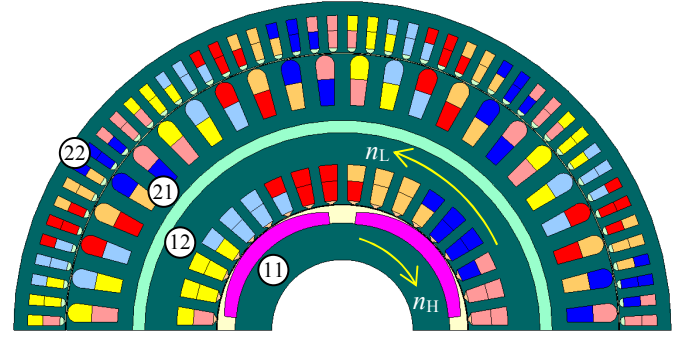


Fig. 5. Cross section of the wind generator with two counter rotating rotors: ⑪ - field armature of PMSG, ⑫ - coil armature of PMSG, ⑪ - primary of IG, ⑫ - secondary of IG.

Table I contains the main geometrical data of the IG and of the PMSG.

TABLE I. MAIN GEOMETRICAL DATA OF THE WIND GENERATOR

Low Speed IG (300 rpm)		High Speed PMSG (600 rpm)	
Stator outer diameter [mm]	326	Stator outer diameter [mm]	196
Stator inner diameter [mm]	275	Stator inner diameter [mm]	125
Height of stator tube [mm]	184	Height of stator tube [mm]	184
Rotor outer diameter [mm]	273.8	Rotor outer diameter [mm]	123.8
Rotor inner diameter [mm]	208	Rotor inner diameter [mm]	70
Airgap [mm]	0.6	Airgap [mm]	0.6
Rotor slots number Z_{21}	48	Slots number Z_{12}	36
Stator slots number Z_{22}	96		

B. FEM Numerical Model

The estimation of the generator behaviour was carried out by solving several transient electromagnetic field circuit coupled problems, at different loads. The rotation of the mobile armatures was taken into account using a movement with constant time step.

For each time step, the non-linear magnetic field was computed by using the following partial differential equation based on the magnetic vector potential \mathbf{A} :

$$\text{curl}[\nu(\mathbf{B}) \cdot \text{curl} \mathbf{A}] = \mathbf{J} + \text{curl}[(\nu(\mathbf{B})) \cdot \mathbf{B}_r], \quad (14)$$

where ν represents the magnetic reluctivity, \mathbf{J} the current density, and \mathbf{B}_r the remnant magnetic flux density of the permanent magnets.

The computation domain was reduced, based on the existing symmetries, to half of the generator cross-section, Fig. 6. The finite element mesh was built in such a way to obtain a refined discretization in the area of the two air-gaps of the generator. The movement of the rotor was modelled with the help of two gliding surfaces placed in the generator air-gaps (details shown in the yellow squares in Fig. 6).

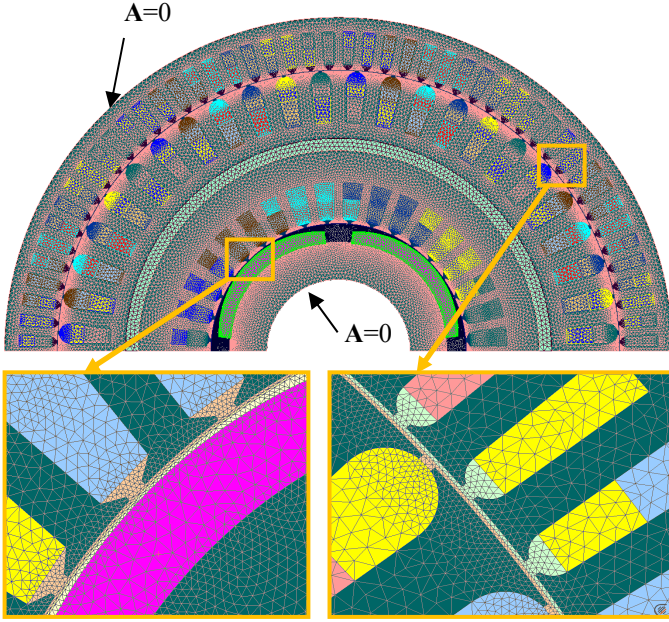


Fig. 6. Mesh of the domain and boundary conditions.

On the outer contour a Dirichlet condition was imposed (i.e. the magnetic field is tangent to that boundary), while on the radial boundaries a periodic condition was enforced.

The electrical circuit associated to the field problem, Fig. 7, has three areas, one corresponding to the PMSG, one to the IG and another one depicting the load. The electric circuit of the winding of one of the three phases $P \in \{U, V, W\}$ comprises BP1_{ij} and BP2_{ij} components that correspond to the active coil sides (the leaving and returning sides), while RP_{ij} and LsP_{ij} are the resistance and the inductance of the end-coil segment and RFE_{Pij} is the resistance equivalent to iron losses. The total resistance of a phase winding is given by RP_{ij}. The load impedance components are represented by RP_L and LP_L, respectively. The numerical values of the circuit components are shown in Table II.

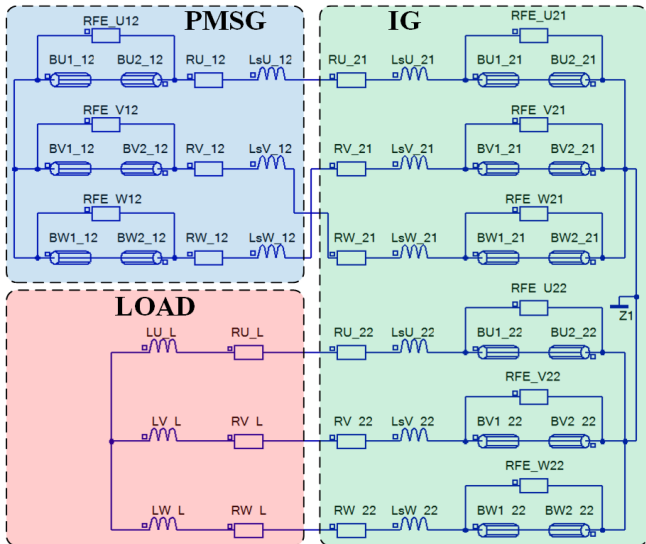


Fig. 7. Electric circuit associated to field problem.

TABLE II. ELECTRIC CIRCUIT COMPONENTS VALUES

RP_12	1.8	[Ω]	RP_21	2.96	[Ω]
LsP_12	3.58	[mH]	LsP_21	2.1	[mH]
RFE_12	3585	[Ω]	RFE_21	2709	[Ω]
RP_L	19.66	[Ω]	RP_22	1.55	[Ω]
LP_L	14.69	[mH]	LsP_22	0.74	[mH]
			RFE_22	4512	[Ω]

C. Analysis of the Generator Operation under Load Condition

At first, the wind generator operation is investigated under rated load, considering the two rotors spinning at their constant rated speeds.

The field model was used for sizing and optimizing the magnetic circuits, in order to obtain the magnetic stress within suitable limits, Fig. 8. For the considered load value, the PMSG line voltage obtained was $U_{12} = 451$ V and the current flowing inside the interconnected windings of the two generators was $I_{12} = I_{21} = 10.36$ A. The waveforms are shown in Fig. 9.

The wind generator line voltages and the currents absorbed by the considered RL load are represented in Fig. 10. Their effective values are: $U_{22} = 402.5$ V and $I_{22} = 10.9$ A.

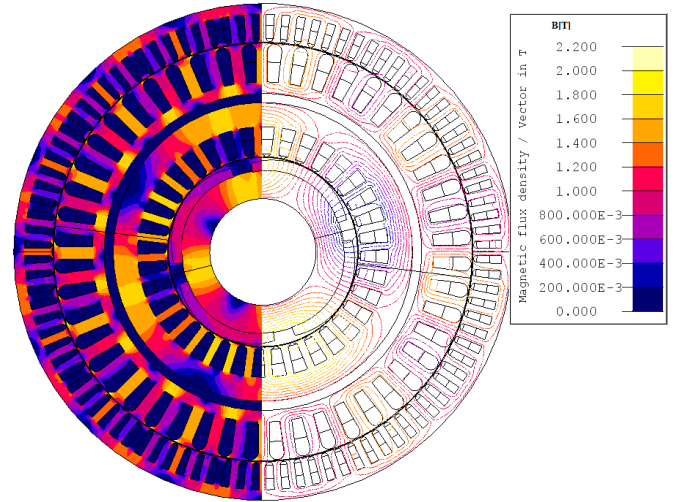


Fig. 8. The magnetic field distribution at rated load operation.

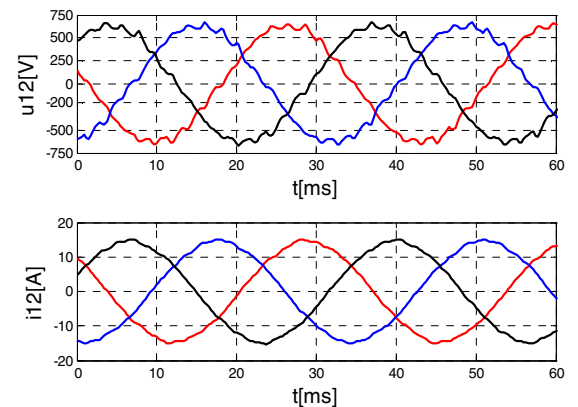


Fig. 9. Output voltage and load current of PMSG.

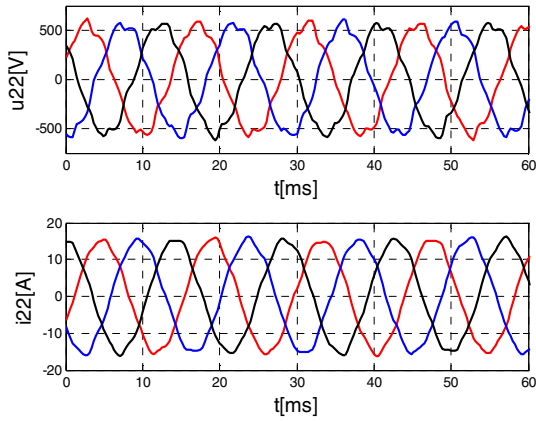


Fig. 10. Output voltage and load current of wind generator.

In the diagram shown in Fig. 11 P_{m1} represents the mechanical power received from the high speed turbine and P_{m2} represents the power received from the low speed wind turbine. In the lower part of the diagram are shown the Joule and iron losses produced in the armature of the PMSG, (12), and in the primary, (21), and secondary armatures, (22), of the IG. The active power provided by PMSG, which is denoted by P_{12} , is equal to the power P_{21} received by the IG. The electromagnetic power at the IG air-gap level is denoted by P_{em2} , and the output power transmitted to the load with P_L .

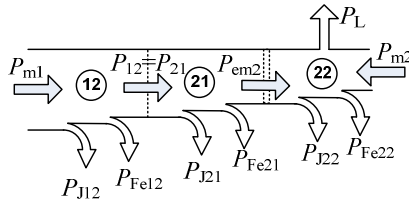


Fig. 11. Chart of the active powers balance.

The power values shown in Fig. 11 were obtained from the numerical model at the rated operation and are specified in Table III. Based on these values, the rated efficiency was estimated as $\eta = 75.77\%$.

TABLE III. POWERS VALUES OF WIND GENERATOR

P_{m1}	P_{m2}	P_{12}	P_{21}	P_{em2}	P_L
[W]	[W]	[W]	[W]	[W]	[W]
5076	4359	4436	4436	3412	7022
P_{J12}	P_{Fe12}	P_{J21}	P_{Fe21}	P_{J22}	P_{Fe22}
[W]	[W]	[W]	[W]	[W]	[W]
580	59	954	58	553	41

V. CONCLUSIONS

This paper presents a FE analysis of a special wind generator with two counter-rotating rotors. The proposed generator operates as a two in one machine and includes a PMSG and an IG in cascade connection. The main advantage of this solution is the absence of the sliding contacts which offers a higher mechanical reliability.

The numerical model allowed the generator design and the estimation of its overall performance at the rated operation point. The numerical results revealed a moderate efficiency of the generator, mainly due to the PMSG that must provide the reactive power to the IG through a reactive electric current, which generates additional Joule losses. However, the reduced efficiency is compensated by the advantage of a smaller, more efficient double propeller wind turbine.

To integrate such a generator into a wind conversion system with a higher overall efficiency, a special attention should be paid to power distribution among the two generators and to the correlation with the wind turbine features.

ACKNOWLEDGMENT

This paper was elaborated in the framework of the Partnership Programme – PNCDI II, financed by MEN - UEFISCDI, project no. 41/2014.

REFERENCES

- [1] Y. Duan, R.G. Harley, "Present and future trends in wind turbine generator designs," in Proc. of *Power Electronics and Machines in Wind Applications (PEMWA 2009)*, June 2009.
- [2] V.V. Mehre, S.G. Desai, D.S. Bankar, "Analysis of a Doubly Fed induction generator based wind farm," in Proc. of *IEEE Technological Innovations in ICT for Agriculture and Rural Development*, July 2016.
- [3] N. Karakasis, N. Jabbour, E. Tsioumas, "Efficiency increase in a wind system with Doubly Fed Induction Generator," in Proc. of *42nd IEEE Annual Conference of the Industrial Electronics Society*, October 2016.
- [4] L. Barote, C. Marinescu, "Modeling and Operational Testing of an Isolated Variable Speed PMSG Wind Turbine with Battery Energy Storage," *Advances in Electrical and Computer Engineering Journal*, vol. 12, issue 2, pp. 81-88, 2012.
- [5] A. Damiano, G. Gatto, I. Marongiu, A. Serpi, "A multi-phase PM synchronous generator torque control for direct-drive wind turbines", *International Symposium on Power Electronics, Electrical Drives, Automation and Motion (SPEEDAM)*, pp. 962 – 968, 2012.
- [6] M. Popescu, G. Oprina, A. Mituletu, S. et al., "Aspects regarding the application of electric generators to wind energy conversion using counter rotating turbines", in Proc. of the *IEEE International Symposium on Advanced Topics in Electrical Engineering (ATEE)*, pp. 1 - 4, 2013.
- [7] P. C. Sai, S. Richa, R. Yadav, R. Nihar Raj, G. R. K. Gupta, "Design and simulation of high efficiency counter-rotating Vertical Axis Wind Turbine arrays", in Proc. of *Int. Conference and Utility Exhibition on Green Energy for Sustainable Development (ICUE)*, pp. 1 - 9, 2014.
- [8] M. Agung Bramantya, Luqman Al Huda, "An experimental study on the mechanics power of counter rotating wind turbines model related with axial distance between two rotors" in Proc. of the *Int. Annual Engineering Seminar (InAES)*, pp. 212 - 217, 2016.
- [9] Yosua Heru Irawan, M. Agung Bramantya, "Numerical simulation of the effect of axial distance between two rotors in counter-rotating wind turbines", in Proc. of the *International Conference on Science and Technology-Computer (ICST)*, pp. 1 - 5, 2016.
- [10] Y. Debleser and Jeumont Industrie, "Wind turbine with counter rotating rotors", US Patent No. 6504260, 2003.
- [11] S.N. Jung, T.-S. No, K.-W. Ryu, "Aerodynamic performance prediction of a 30 kW counter-rotating wind turbine system", *Renewable Energy*, vol. 30, 2005, pp.631-644.
- [12] A. Ozbay, W. Tian, H. Hu, "Experimental investigation on the wake characteristics and aeromechanics of dual-rotor wind turbines", *J. Eng Gas Turbines Power* 2016;138(4).
- [13] S. Lee, H. Kim, S. Lee, "Analysis of aerodynamic characteristics on a counter-rotating wind turbine", *Current Applied Physics*, vol. 10, pp. 339-342, 2010.
- [14] CEDRAT: "User guide Flux® 11", 2012.